Supporting Information
Benchmarking Electro-organic Reaction Performance via Multi-dimensional Bayesian Optimization with Cross-Phase Categorical-Continuous Variable Sets

Luhan Dai[1], Pan Ran[1], Fangyuan Wang[1], Aoqian Qiu[1], Tianshu Liu[1], Jun Li[1], Chongyue Luo[1], Yuhao Zhai[1], Jin Xie[1], Mengning Ding[1]*

[1] Key Laboratory of Mesoscopic Chemistry, State Key Laboratory of Coordination Chemistry, State Key Laboratory of Analytical Chemistry for Life Sciences, School of Chemistry and Chemical Engineering, Nanjing University, Nanjing, Jiangsu, 210023, China

Bayesian Optimization

Principle of Bayesian optimization. Bayesian optimization operates by constructing a probabilistic model of the objective function based on prior evaluations, which is then iteratively updated as new data is acquired. The core principle of Bayesian optimization involves the use of a surrogate model, often a Gaussian Process (GP), to estimate the value of the objective function at unobserved points in the search space. The model provides a distribution over possible functions, which captures both the predicted mean and uncertainty of the function at each point. This probabilistic framework allows for both exploration (sampling in areas where the model is uncertain) and exploitation (sampling in areas where the model predicts high objective function values), thereby efficiently navigating the search space. The process begins with an initial set of function evaluations, which serve to train the surrogate model. After each evaluation, the model is updated, and an acquisition function is used to determine the next point to evaluate. Acquisition functions, such as Expected Improvement (EI), Probability of Improvement (PI), or Upper Confidence Bound (UCB), quantify the trade-off between exploring uncertain areas and exploiting regions predicted to yield high values. The acquisition function is maximized to select the next sample point, which is then evaluated, and the cycle continues until a stopping criterion is met, such as a budget of evaluations or convergence to an optimal solution.

Expected Hypervolume Improvement (EHVI). EHVI measures the expected improvement in the hypervolume, which is a metric that quantifies the volume dominated by a set of solutions in the objective space. The hypervolume represents the quality of the solution set in terms of the trade-offs between multiple objectives, with a larger hypervolume corresponding to a set of solutions that dominate a greater portion of the objective space. EHVI is designed to guide the optimization process by selecting new candidate points that are expected to improve the hypervolume, thereby moving closer to the Pareto front of optimal trade-offs between the objectives. The principle behind EHVI lies in balancing exploration and exploitation in the search for optimal solutions. At each iteration, the acquisition function evaluates the expected change in hypervolume by considering the current surrogate model of the objective functions and the predicted improvement in the objective space. This allows the algorithm to prioritize areas where a significant improvement in the hypervolume is expected, even if those areas have not been thoroughly explored yet, while also focusing on regions that are likely to yield high-quality solutions.

SHAP value analysis. SHAP value represents the average contribution of a given feature across all possible combinations of features. SHAP value calculates the difference in model predictions when a feature is included or excluded from the model, averaged across all possible feature combinations. This provides a comprehensive and unbiased measure of the feature's contribution, considering not only its direct effect but also the interactions with other features. In practice, SHAP value analysis can be used to understand both global and local feature importance. Global importance refers to the overall contribution of each feature to the model's predictions across the entire dataset, while local importance focuses on the specific contribution of each feature for individual predictions. This dual-level insight is crucial for explaining model behavior in a manner that is interpretable and actionable. For example, by analyzing the SHAP values, researchers can identify which features most strongly influence the model's predictions, detect potential biases, and even uncover unexpected patterns or relationships in the data.

Code availability. All codes were written based on an open-source Bayesian optimization package: OpenBox (the source can be found on "https://github.com/PKU-DAIR/open-box"). Our code was slightly adjusted from the official file "quick_example.py". Full codes are packed in an individual file named "code.zip"

Mono-objective Tetralin Optimization

Full name and unit for experimental parameters: CatL: catalyst loading (mg); SubC: substrate concentration (M), SolR: ration of ACN/H_2O; t: time (h); E: applied potential (V vs Ag/AgCl); Ani.: anions for electrolytes; Cat.: cation for electrolytes.

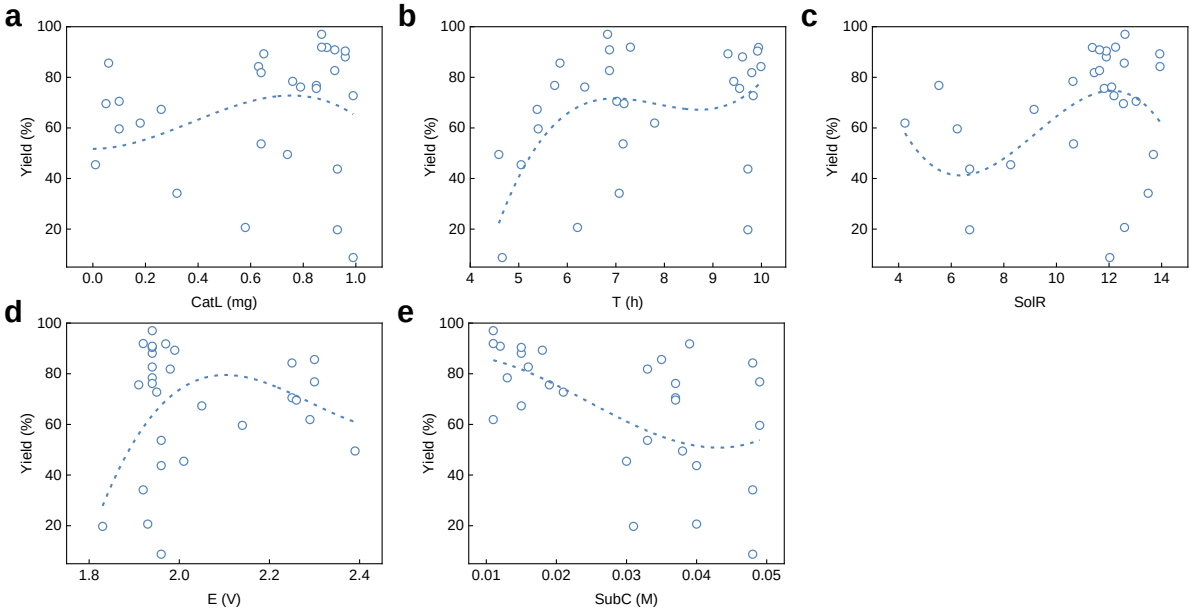

Figure S1. Yield values for different parameters within defined parameter intervals for mono-objective optimization for electrocatalytic tetralin C–H activation. Total five parameters are exhibited.

Multi-objective Tetralin Optimization

Full name and unit for experimental parameters: CatL: catalyst loading (mg); SubC: substrate concentration (M), SolR: ration of ACN/H_2O; t: time (h); E: applied potential (V vs Ag/AgCl); Ani.: anions for electrolytes; Cat.: cation for electrolytes.

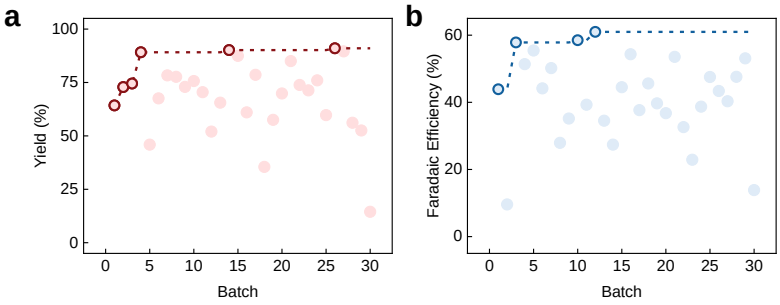

Figure S2. Yield and FE optimization curve with the increasing batches. The optimal results are shown in dashed line.

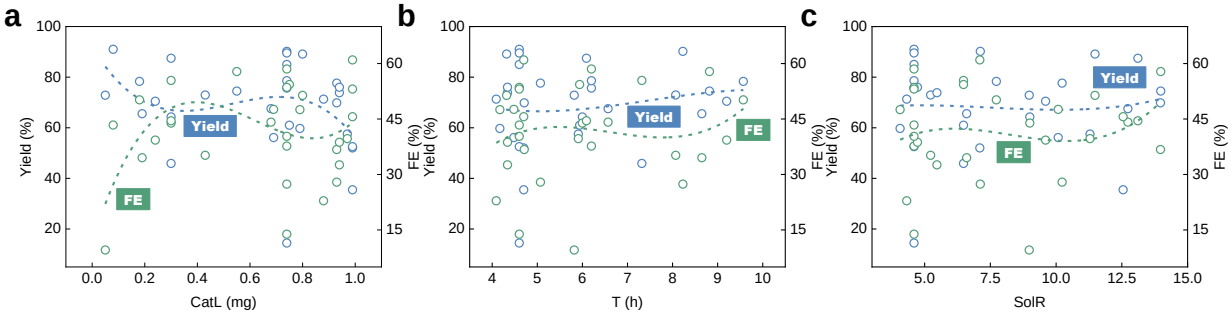

Figure S3. Yield and FE values for different parameters within defined parameter intervals for multi-objective optimization for electrocatalytic tetralin C–H activation. Total three parameters are exhibited, with other two parameters exhibited in the main text.

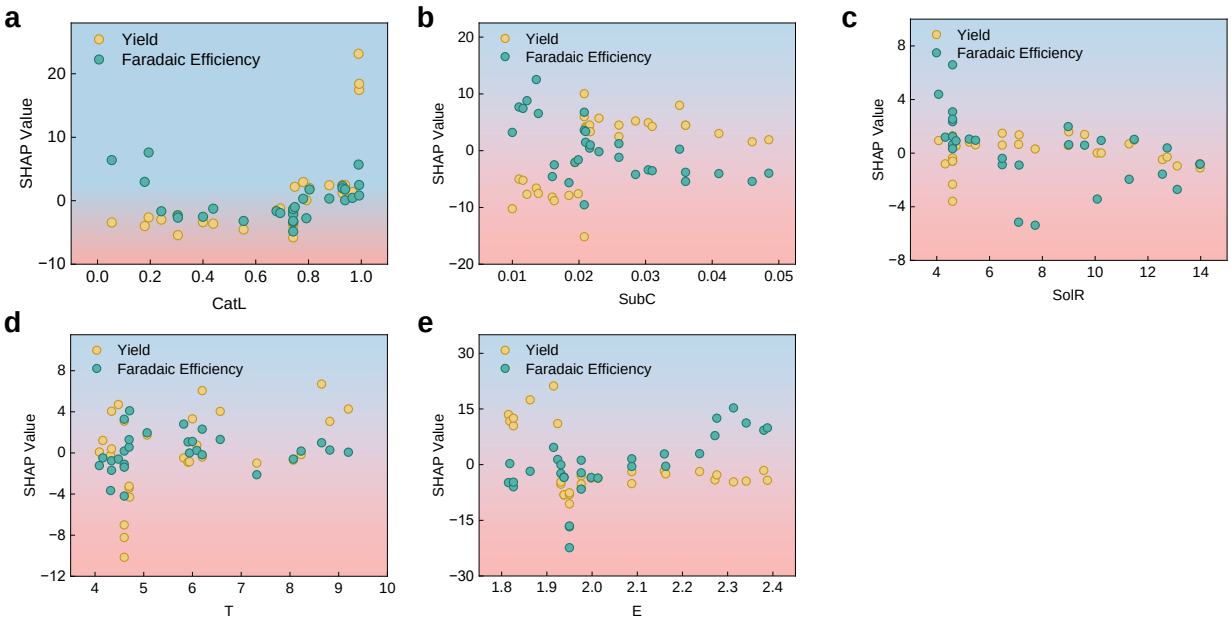

Figure S4. SHAP values for different parameters within defined parameter intervals for multi-objective optimization for electrocatalytic tetralin C–H activation. Total five parameters are exhibited, namely catalyst loading, concentration of substrate, ratio of solvents, time and potential.

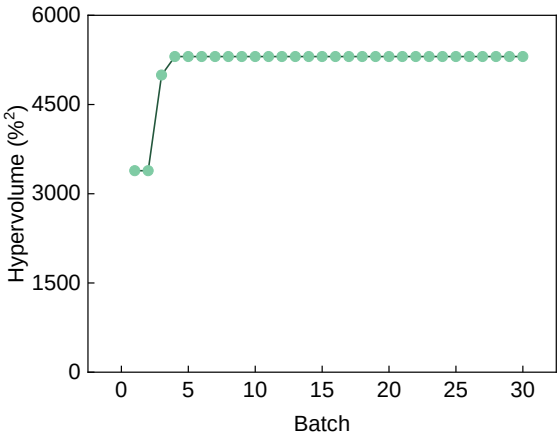

Figure S5. Hypervolume indicated the performance improvement for electrocatalytic tetralin C–H activation.

Multi-objective Olefin Optimization

Full name and unit for experimental parameters: CatL: catalyst loading (mg); H_2OL: water ratio of entire solvent (%); SubC: substrate concentration (M), EleL: electrolyte loading (M); t: time (h); E: applied potential (V vs Ag/AgCl); Ani.: anions for electrolytes.

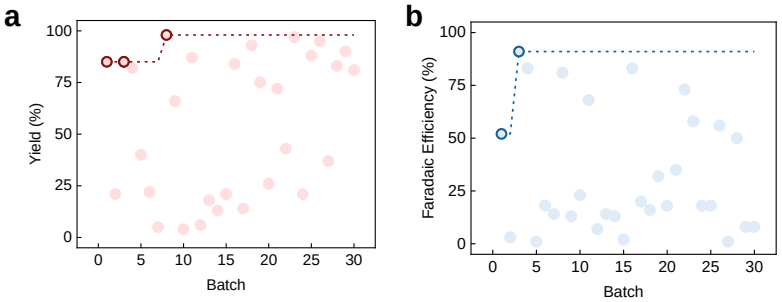

Figure S6. Yield and FE optimization curve with the increasing batches. The optimal results are shown in dashed line.

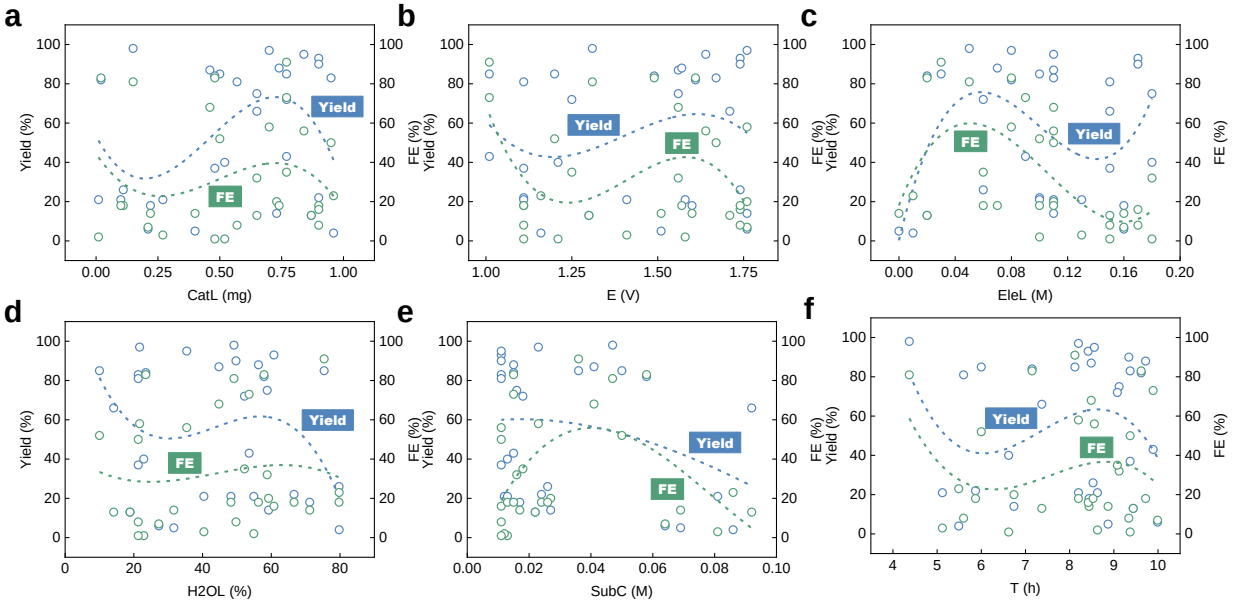

Figure S7. Yield and FE values for different parameters within defined parameter intervals for multi-objective optimization for electrocatalytic olefin epoxidation. Total six parameters are exhibited.

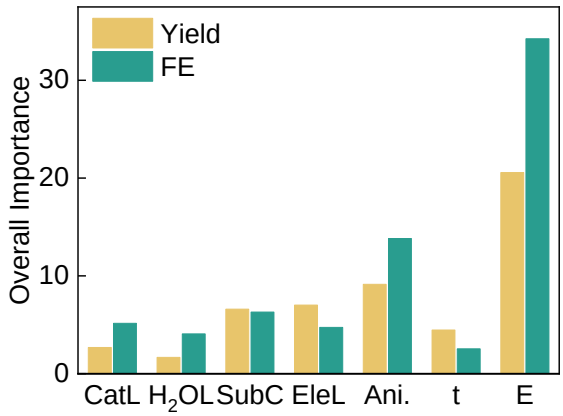

Figure S8. Overall importance indicated by SHAP value for separate parameters upon their valuing range of electrocatalytic olefin epoxidation reaction, and the value for two objectives (yields and FEs) are shown in different colors

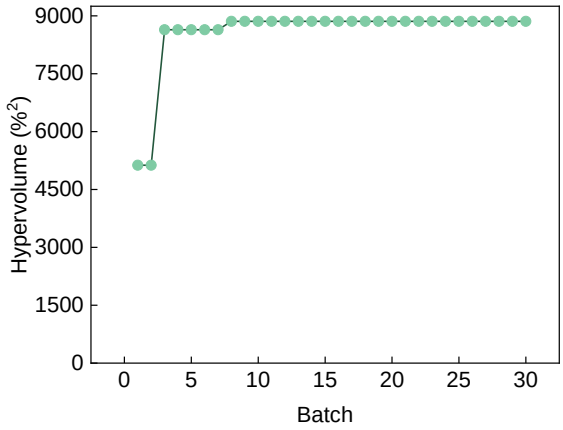

Figure S9. Hypervolume indicated the performance improvement for electrocatalytic olefin epoxidation reaction.

Multi-objective Oxidative Cleavage Optimization

Full name and unit for experimental parameters: Cat: catalyst species; CatL: catalyst loading (mg); SubC: substrate concentration (M), H_2OL: water ratio of entire solvent (%); t: time (h); E: applied potential (V vs Ag/AgCl).

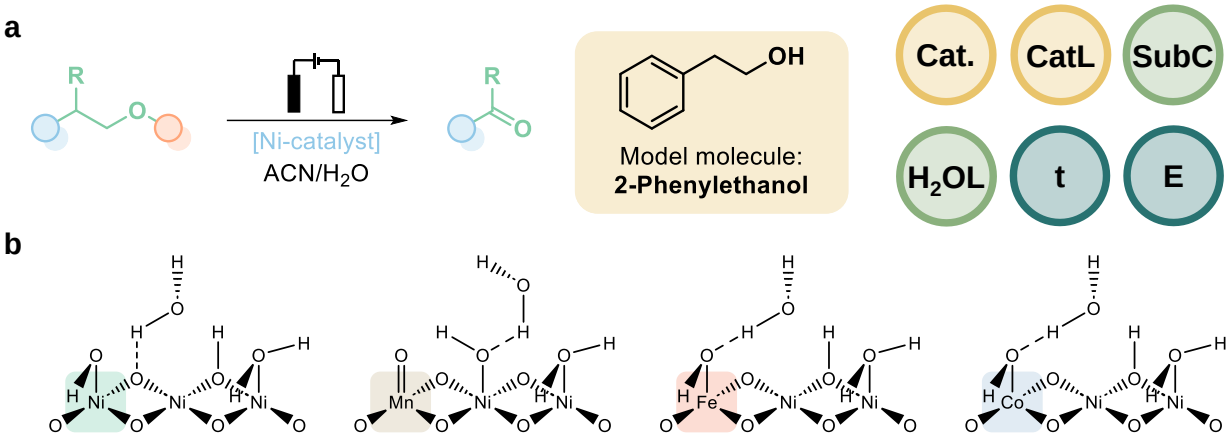

Figure S10. Application of Bayesian framework on the optimization of electrocatalytic oxidative C–C cleavage reaction. a. Illustration of the electrocatalytic oxidative C–C cleavage reaction assisted by partial water oxidation (left panel). Key parameters involved in the optimization process (right panel). **b.** Choice of catalysts with an additional corresponding parameter added to the chemical space based on expert-informed knowledge. Four catalyst options were provided for optimization (elementary Nickel hydroxide and three potential metal doping).

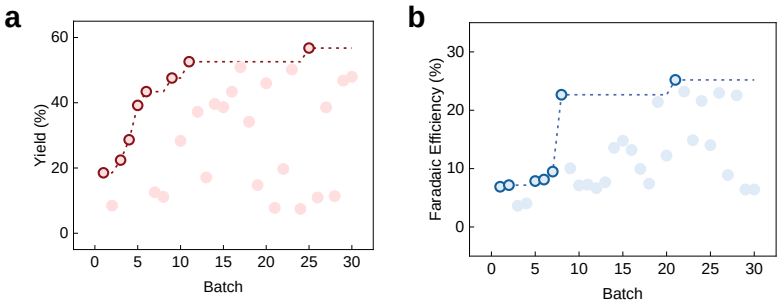

Figure S11. Yield and FE optimization curve with the increasing batches. The optimal results are shown in dashed line.

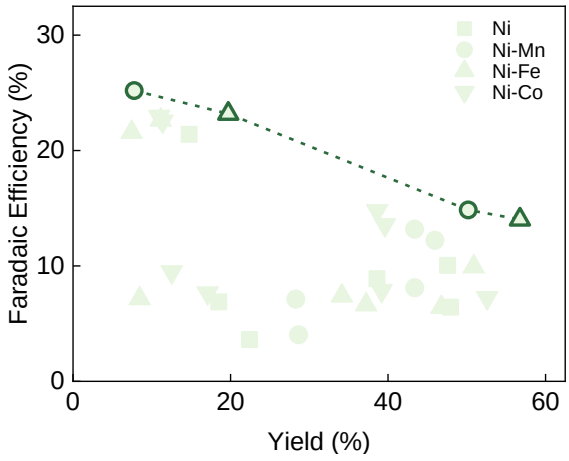

Figure S12. Pareto front emphasized through bold dashed line in two-dimensional graph, with different shapes representing four different catalysts options.

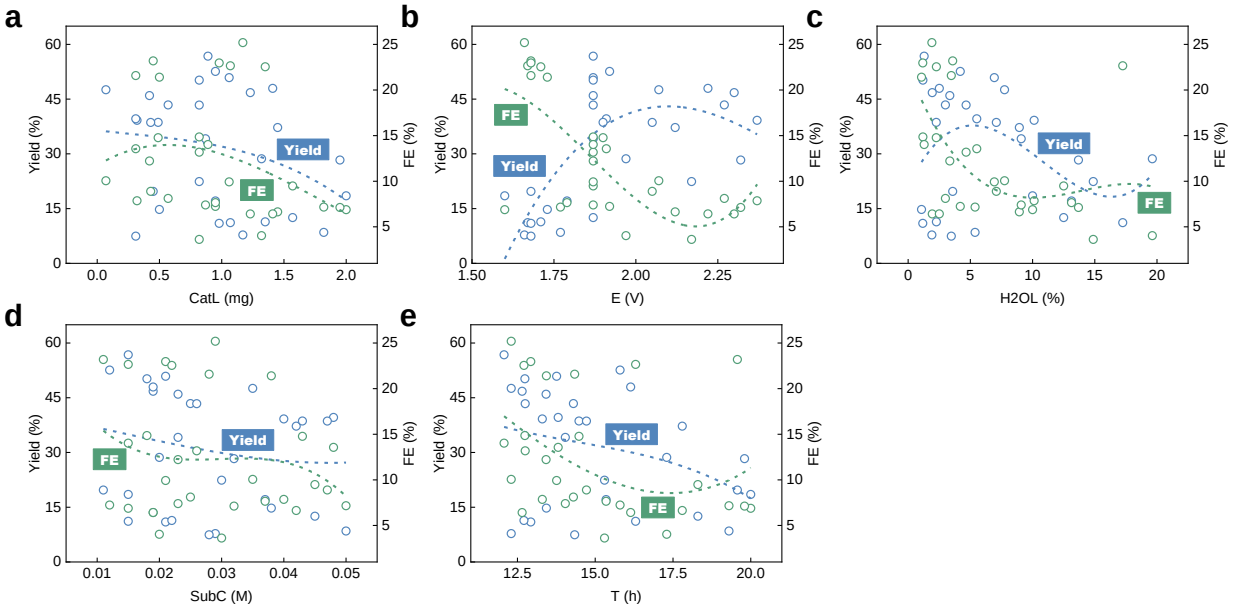

Figure S13. Yield and FE values for different parameters within defined parameter intervals for multi-objective optimization for electrocatalytic olefin epoxidation. Total five parameters are exhibited.

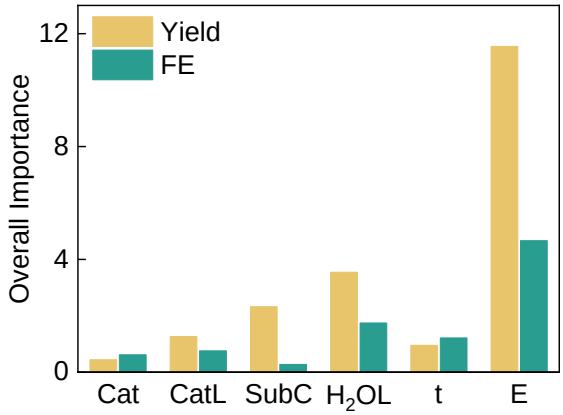

Figure S14. Overall importance indicated by SHAP value for separate parameters upon their valuing range of electrocatalytic oxidative C–C cleavage reaction, and the value for two objectives (yields and FEs) are shown in different colors

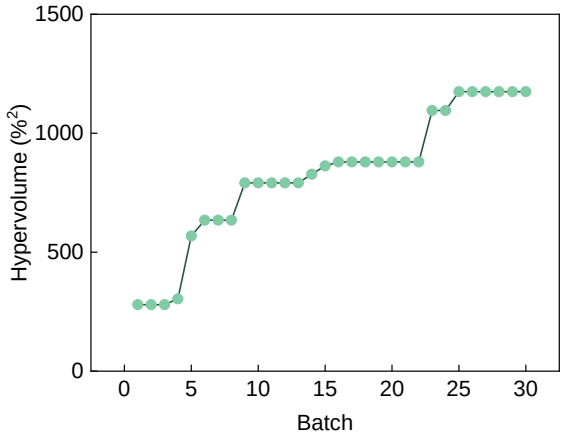

Figure S15. Hypervolume indicated the performance improvement for electrocatalytic oxidative C–C cleavage reaction.

Carbon-carbon bond cleavage (Figure **S10a**) represents another practically important model reaction[1] that follows a distinct oxidative pathway. As C−C bonds are highly stable, precise catalyst (surface) design is often required to improve reaction yield and product selectivity. Based on the analysis of numerous reports[1-7] focusing on the electrocatalytic C−C cleavage, it can be hypothesized that transition metal doping in Ni-based catalysts (which can be generally represented by Ni oxyhydroxide catalysts) can subtly adjust the electronic structure and/or surface micro-kinetics of the catalyst, thereby lowering the activation energy and promote the electro-oxidative C−C cleavage. To date, systematic analysis on the catalyst design is still required for further development of effective oxidation-based cleavage transitions of various types of organic/polymer/biomass substrates. For this aim, four representative catalyst options were investigated in our Bayesian optimizations, including pristine Nickel hydroxide

(abbreviated as Ni-Cat.), and Ni-Cat. Incorporated with Mn, Fe, and Co doping (abbreviated as Ni-Mn Cat., Ni-Fe Cat. and Ni-Co Cat., respectively). These doping metals were selected for their proximity to Ni on the periodic table and based on the inputs from literature, whereas additional composition options can be added based on further experimental findings or new mechanistic insights. We first provide a microscopic depiction of these catalysts in Figure **S10b**, where the metal atom on the left represents an active site. Subsequently, we deliberately set the reaction time parameter to a limited range (between 12 to 20 hours) that is considerably shorter than the typically reported values (often exceeding 40 hours). After 30 batches of Bayesian optimization, the selected catalysts did establish certain reaction conditions that do not require extended reaction time yet provide superior yield with acceptable FE (given the generally poor FE performance reported in literature). The hypervolume analysis demonstrates stable optimization throughout the modeling process. On the Pareto front, three optimal conditions favor a 12-hour reaction time, confirming the success search of kinetically faster conditions using our strategy. This example indicates the promising potential of Bayesian optimization to systematically adjusting reaction parameters and achieve optimal conditions when external restrictions on certain parameters are desired (in this work, the reaction time is to be reduced for cost considerations).

Similarly, individual experimental results and the Pareto front are included in Figures S10c-e (also see Table **S7**), illustrating a distinct trend in objective values to the optimization processes in other reactions. Under the optimized conditions, the optimal yield of benzaldehyde represents a significant improvement over typical reported yield. According to the Pareto front, the Ni-Mn and Ni-Fe catalysts exhibit superior performance compared to the other two catalyst options. A closer examination of the Pareto front points in Figure S10f shows a slower decline in FE (from 25% to 14%). In contrast, the reaction yield significantly increases to 57%, suggesting that a slow reaction rate and presumably inevitable side reactions during C–C bond activation. Adjusting the catalyst can facilitate substrate adsorption, enhancing selectivity for the desired product and reducing the likelihood of over-oxidation. In contrast, other catalysts generally exhibit poor performance, with cobalt identified as a poisoning agent for this reaction. Again, electrochemical potential is clearly the most influential parameter according to the importance analysis (Figure **S11**), with yield showing a greater potential dependence as compared to FE. This heightened sensitivity may be attributed to the challenging adsorption and activation of phenylethyl alcohol. For similar reasons, water content is another crucial factor for both yield and FE, as the lower level of water content may be key to help mitigate side reactions.

Multi-objective Oxidative Cleavage Optimization

Full name and unit for experimental parameters: Cat: catalyst species; CatB: catalyst supporting material; SubC: substrate concentration (M), BasC: base concentration in solvent (M); Cat.: cation for electrolyte; t: time (h); E: applied potential (V vs Ag/AgCl).

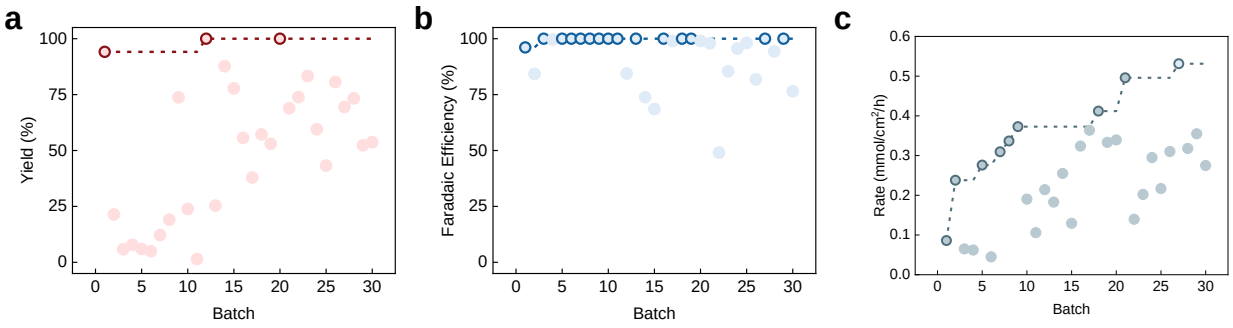

Figure S16. Yield, FE and rate optimization curve with the increasing batches. The optimal results are shown in dashed line.

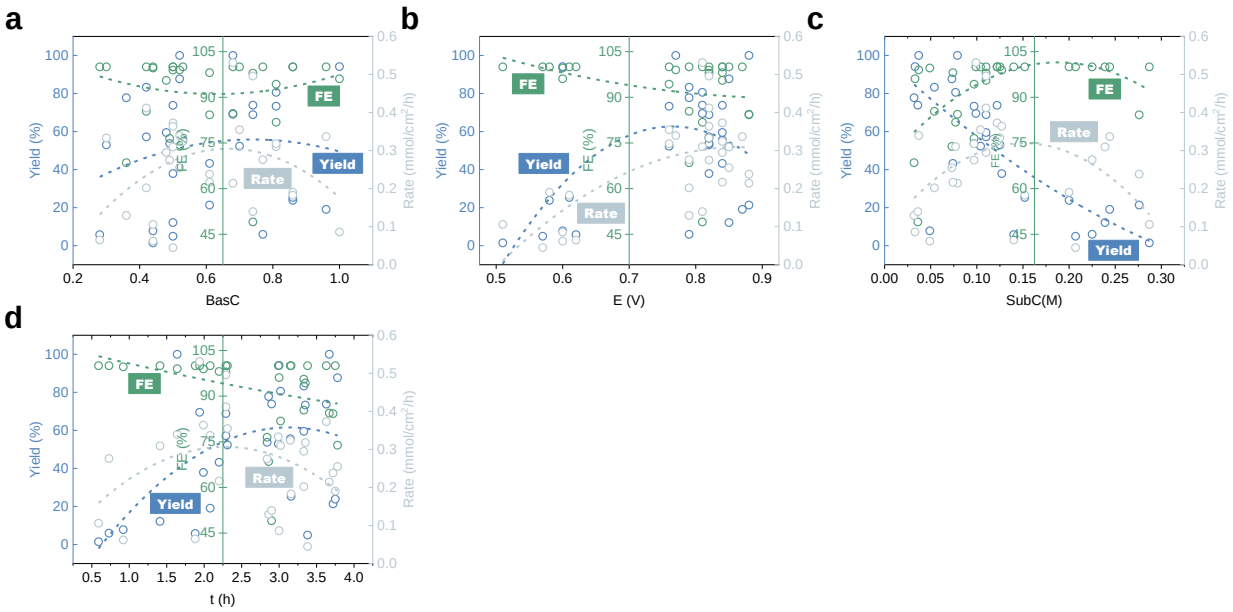

Figure S17. Yield, FE and rate values for different parameters within defined parameter intervals for multi-objective optimization for electrocatalytic amine oxidation. Total four parameters are exhibited.

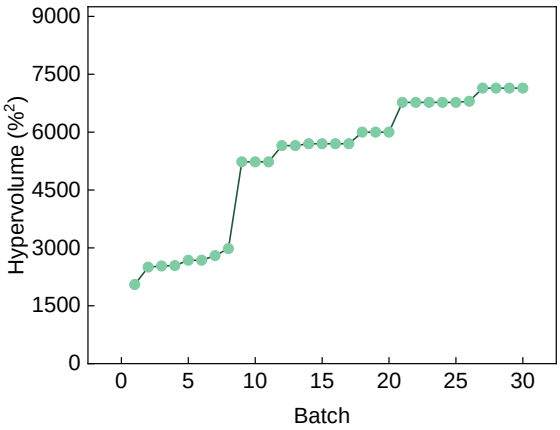

Figure S18. Hypervolume indicated the performance improvement for electrocatalytic amine oxidation reaction.

Conditions of Bayesian Optimization

Table S1. Batch conditions of mono-objective optimization for electrocatalytic tetralin C–H activation.

Entry	CatL (mg)	SubC (M)	SolR	Cation	Anion	T (h)	E (V)	Yield (%)
1	0.00	0.04	5.60	Li^+	ClO_4^-	5.10	1.91	0
2	0.99	0.02	12.19	Bu_4N^+	BF_4^-	9.83	1.95	72.74
3	0.85	0.05	5.53	Li^+	BF_4^-	5.74	2.30	76.79
4	0.18	0.01	4.24	Li^+	ClO_4^-	7.80	2.29	61.9
5	0.06	0.03	12.58	Li^+	BF_4^-	5.85	2.30	85.59
6	0.63	0.05	13.94	Bu_4N^+	ClO_4^-	9.99	2.25	84.24
7	0.10	0.04	13.03	Bu_4N^+	BF_4^-	7.02	2.25	70.49
8	0.85	0.02	11.82	Bu_4N^+	BF_4^-	9.55	1.91	75.6
9	0.32	0.05	13.49	Li^+	ClO_4^-	7.07	1.92	34.16
10	0.58	0.04	12.59	Bu_4N^+	BF_4^-	6.21	1.93	20.62
11	0.26	0.02	9.15	Bu_4N^+	BF_4^-	5.38	2.05	67.3
12	0.05	0.04	12.55	Li^+	BF_4^-	7.17	2.26	69.58
13	0.74	0.04	13.69	Bu_4N^+	ClO_4^-	4.59	2.39	49.49
14	0.64	0.03	10.65	Bu_4N^+	BF_4^-	7.15	1.96	53.67
15	0.89	0.04	11.37	Bu_4N^+	BF_4^-	9.94	1.97	91.78
16	0.99	0.05	12.03	Li^+	BF_4^-	4.66	1.96	8.74
17	0.10	0.05	6.23	Li^+	BF_4^-	5.40	2.14	59.62
18	0.96	0.02	11.90	Li^+	ClO_4^-	9.61	1.94	88.07
19	0.93	0.03	6.70	Bu_4N^+	BF_4^-	9.72	1.83	19.72
20	0.01	0.03	8.26	Bu_4N^+	ClO_4^-	5.05	2.01	45.43
21	0.65	0.02	13.93	Bu_4N^+	ClO_4^-	9.31	1.99	89.27
22	0.64	0.03	11.44	Bu_4N^+	ClO_4^-	9.80	1.98	81.82
23	0.93	0.04	6.70	Bu_4N^+	ClO_4^-	9.72	1.96	43.72
24	0.96	0.02	11.90	Li^+	ClO_4^-	9.92	1.94	90.38
25	0.87	0.01	12.61	Bu_4N^+	BF_4^-	6.83	1.94	96.99
26	0.92	0.02	11.64	Li^+	ClO_4^-	6.87	1.94	82.66
27	0.76	0.01	10.63	Bu_4N^+	BF_4^-	9.43	1.94	78.38
28	0.92	0.01	11.64	Li^+	ClO_4^-	6.87	1.94	90.85
29	0.79	0.04	12.10	Li^+	BF_4^-	6.36	1.94	76.16
30	0.87	0.01	12.25	Li^+	ClO_4^-	7.30	1.92	91.91

Table S2. Batch conditions of multi-objective optimization for electrocatalytic tetralin C–H activation.

Entry	CatL (mg)	SubC (M)	SolR	Cation	Anion	T (h)	E (V)	Yield (%)	FE (%)
1	0.30	0.026	9.00	Bu_4N^+	ClO_4^-	6.00	2.00	64.27	43.89
2	0.05	0.026	8.98	Bu_4N^+	BF_4^-	5.82	2.31	72.85	9.58
3	0.55	0.046	13.98	Li^+	ClO_4^-	8.82	2.01	74.50	57.83
4	0.80	0.016	11.48	Bu_4N^+	ClO_4^-	4.32	2.16	89.13	51.37
5	0.30	0.036	6.48	Li^+	BF_4^-	7.32	1.86	45.90	55.42
6	0.68	0.041	12.73	Li^+	ClO_4^-	6.57	2.24	67.54	44.14
7	0.18	0.021	7.73	Bu_4N^+	BF_4^-	9.57	1.94	78.31	50.18
8	0.93	0.011	10.23	Li^+	ClO_4^-	5.07	2.09	77.64	27.93
9	0.43	0.031	5.23	Bu_4N^+	BF_4^-	8.07	2.39	72.92	35.17
10	0.74	0.028	4.60	Li^+	BF_4^-	6.20	1.98	75.68	58.51
11	0.24	0.048	9.60	Bu_4N^+	ClO_4^-	9.20	2.28	70.47	39.28
12	0.99	0.018	7.10	Li^+	BF_4^-	4.70	1.83	52.02	60.98
13	0.19	0.019	6.60	Bu_4N^+	ClO_4^-	8.65	1.93	65.54	34.52
14	0.74	0.014	7.12	Li^+	BF_4^-	8.23	1.98	90.17	27.39
15	0.30	0.021	13.11	Li^+	BF_4^-	6.09	1.94	87.45	44.51
16	0.75	0.036	6.48	Bu_4N^+	BF_4^-	5.94	2.00	61.00	54.32
17	0.74	0.020	4.60	Li^+	BF_4^-	6.20	1.98	78.58	37.68
18	0.99	0.022	12.55	Li^+	BF_4^-	4.70	1.83	35.48	45.62
19	0.97	0.014	11.29	Li^+	BF_4^-	5.91	1.81	57.51	39.69
20	0.93	0.022	13.97	Bu_4N^+	BF_4^-	4.71	2.09	69.84	36.75
21	0.74	0.021	4.60	Li^+	BF_4^-	4.60	1.95	85.00	53.54
22	0.94	0.016	5.47	Bu_4N^+	BF_4^-	4.34	2.34	73.83	32.60
23	0.88	0.012	4.32	Li^+	ClO_4^-	4.09	2.38	71.31	22.89
24	0.94	0.030	4.73	Li^+	ClO_4^-	4.34	2.27	76.00	38.71
25	0.79	0.023	4.07	Li^+	ClO_4^-	4.17	1.92	59.72	47.53
26	0.08	0.012	4.60	Li^+	BF_4^-	4.60	1.95	91.00	43.37
27	0.74	0.010	4.60	Li^+	ClO_4^-	4.60	1.82	89.55	40.31
28	0.69	0.021	10.08	Li^+	BF_4^-	4.48	1.93	56.13	47.59
29	0.99	0.035	4.60	Li^+	BF_4^-	4.60	1.95	52.53	53.10
30	0.74	0.021	4.60	Li^+	BF_4^-	4.60	1.91	14.45	13.86

Table S3. Batch conditions of mono-objective Bayesian optimization for electrocatalytic indane C-H activation.

Entry	CatL (mg)	SubC (M)	SolR	AddL	Cation	Anion	T (h)	E (V)	Yield (%)
1	0.00	0.026	9.00	0.00	Bu_4N^+	ClO_4^-	6.00	2.16	58.85
2	0.82	0.050	9.74	0.90	Li^+	BF_4^-	6.66	2.36	91.54
3	0.00	0.024	4.41	0.96	Li^+	ClO_4^-	9.25	1.99	73.78
4	0.90	0.036	13.02	0.45	Bu_4N^+	ClO_4^-	9.42	2.03	100
5	0.97	0.025	13.75	0.27	Li^+	BF_4^-	9.08	2.12	100
6	0.23	0.012	10.34	0.17	Li^+	ClO_4^-	9.67	2.23	100
7	0.99	0.035	4.17	0.03	Li^+	BF_4^-	4.45	2.34	4.81
8	0.96	0.048	12.93	0.38	Li^+	BF_4^-	6.04	2.30	66.86
9	0.57	0.029	8.37	0.59	Bu_4N^+	ClO_4^-	9.25	2.03	92.04
10	0.69	0.048	7.74	0.14	Li^+	ClO_4^-	8.56	1.80	10.76

Table S4. Batch conditions of mono-objective Random optimization for electrocatalytic indane C-H activation.

Entry	CatL (mg)	SubC (M)	SolR	AddL	Cation	Anion	T (h)	E (V)	Yield (%)
1	0.00	0.026	9.00	0.00	Bu_4N^+	ClO_4^-	6.00	2.16	58.85
2	0.17	0.045	11.88	0.54	Bu_4N^+	BF_4^-	7.25	1.94	6.86
3	0.60	0.037	6.44	0.31	Bu_4N^+	BF_4^-	9.22	2.31	69.22
4	0.10	0.026	11.11	0.12	Li^+	ClO_4^-	5.67	2.05	73.72
5	0.96	0.014	5.75	0.93	Bu_4N^+	BF_4^-	7.64	2.40	82.04
6	0.52	0.027	7.03	0.45	Bu_4N^+	ClO_4^-	5.64	2.33	80.25
7	0.64	0.032	13.55	0.61	Li^+	BF_4^-	4.86	2.25	60.85
8	0.04	0.014	4.02	0.67	Li^+	BF_4^-	4.60	2.03	80.38
9	0.66	0.042	12.06	0.54	Li^+	BF_4^-	6.73	1.85	5.23
10	0.35	0.016	6.01	0.32	Bu_4N^+	BF_4^-	4.74	2.34	58.47

Table S5. Batch conditions of mono-objective optimization for electrocatalytic 2,3-dihydrobenzofuran C-H activation.

Entry	CatL (mg)	SubC (M)	SolR	AddL	Cation	Anion	T (h)	E (V)	Yield (%)
1	0.30	0.026	9.00	0.00	Bu_4N^+	ClO_4^-	6.00	2.16	12.26
1-2	0.93	0.037	12.16	0.84	Li^+	BF_4^-	7.91	1.86	8.36
1-3	0.91	0.046	4.15	0.20	Bu_4N^+	BF_4^-	8.95	2.38	8.27
1-4	0.20	0.041	13.56	0.63	Bu_4N^+	ClO_4^-	7.14	2.22	9.42
1-5	0.14	0.019	9.79	0.46	Li^+	BF_4^-	6.88	2.09	13.73
2-2	0.97	0.020	7.47	0.09	Li^+	BF_4^-	9.57	1.84	13.04
2-3	0.22	0.028	4.51	1.00	Bu_4N^+	BF_4^-	9.22	2.04	8.2
2-4	0.29	0.027	6.89	0.84	Bu_4N^+	BF_4^-	6.15	2.32	29.05
2-5	0.78	0.046	5.94	0.61	Li^+	BF_4^-	8.85	1.86	4.74
3-2	0.98	0.048	7.11	0.26	Li^+	BF_4^-	9.27	2.34	8.8
3-3	0.86	0.019	12.64	0.69	Bu_4N^+	BF_4^-	9.29	1.87	36.65
3-4	0.55	0.010	8.68	0.97	Li^+	BF_4^-	7.73	1.83	53.76
3-5	1.00	0.048	9.00	0.78	Li^+	ClO_4^-	6.31	2.26	7.84
4-2	0.53	0.049	11.61	0.95	Li^+	BF_4^-	9.79	2.08	4.92
4-3	0.70	0.032	4.10	0.06	Li^+	BF_4^-	4.06	2.23	50.55
4-4	0.75	0.015	4.62	0.80	Li^+	ClO_4^-	5.90	1.83	37.82
4-5	0.10	0.037	12.64	0.24	Li^+	ClO_4^-	7.47	2.12	14.46
5-2	0.95	0.046	11.93	0.94	Li^+	BF_4^-	8.91	1.87	9.82
5-3	0.95	0.034	12.39	0.71	Li^+	BF_4^-	5.71	1.89	26.52
5-4	0.72	0.046	4.00	0.54	Li^+	ClO_4^-	8.45	2.37	12.94
5-5	0.18	0.038	8.49	0.72	Li^+	ClO_4^-	5.07	2.38	12.22
6-2	0.96	0.034	7.43	0.38	Li^+	BF_4^-	9.78	1.83	14.17
6-3	0.62	0.021	4.15	0.89	Li^+	BF_4^-	5.51	1.85	46.06
6-4	0.05	0.042	9.87	0.11	Li^+	BF_4^-	9.92	2.39	15.75
6-5	0.27	0.023	12.16	0.20	Li^+	BF_4^-	8.80	2.12	23.72

Table S6. Batch conditions of multi-objective optimization for electrocatalytic olefin epoxidation reaction.

Entry	CatL (mg)	H_2OL (%)	SubC (M)	EleL (M)	Anion	T (h)	E (V)	Yield (%)	FE (%)
1	0.50	10.00	0.050	0.10	Br^-	6.00	1.20	85%	52%
2	0.27	40.39	0.081	0.13	I^-	5.12	1.41	21%	3%
3	0.77	75.39	0.036	0.03	Br^-	8.12	1.01	85%	91%
4	0.02	57.89	0.058	0.08	Br^-	9.62	1.61	82%	83%
5	0.52	22.89	0.013	0.18	Cl^-	6.62	1.21	40%	1%
6	0.90	66.64	0.024	0.10	Cl^-	5.87	1.11	22%	18%
7	0.40	31.64	0.069	0.00	I^-	8.87	1.51	5%	14%
8	0.15	49.14	0.047	0.05	Br^-	4.37	1.31	98%	81%
9	0.65	14.14	0.092	0.15	I^-	7.37	1.71	66%	13%
10	0.96	79.77	0.086	0.01	I^-	5.49	1.16	4%	23%
11	0.46	44.77	0.041	0.11	Br^-	8.49	1.56	87%	68%
12	0.21	27.27	0.064	0.16	Br^-	9.99	1.76	6%	7%
13	0.22	71.19	0.017	0.16	Cl^-	8.44	1.60	18%	14%
14	0.87	18.88	0.022	0.02	Cl^-	9.44	1.30	13%	13%
15	0.01	54.91	0.012	0.10	Cl^-	8.63	1.58	21%	2%
16	0.48	23.47	0.015	0.02	Br^-	7.15	1.49	84%	83%
17	0.73	59.22	0.027	0.11	Cl^-	6.74	1.76	14%	20%
18	0.90	60.78	0.011	0.17	Cl^-	8.42	1.74	93%	16%
19	0.65	58.81	0.016	0.18	Cl^-	9.12	1.56	75%	32%
20	0.11	79.74	0.026	0.06	Cl^-	8.53	1.74	26%	18%
21	0.77	52.22	0.018	0.06	Cl^-	9.08	1.25	72%	35%
22	0.77	53.56	0.015	0.09	Cl^-	9.89	1.01	43%	73%
23	0.70	21.68	0.023	0.08	Br^-	8.20	1.76	97%	58%
24	0.10	48.25	0.013	0.11	Cl^-	8.20	1.11	21%	18%
25	0.74	56.27	0.015	0.07	Br^-	9.72	1.57	88%	18%
26	0.84	35.40	0.011	0.11	Br^-	8.56	1.64	95%	56%
27	0.48	21.28	0.011	0.15	Cl^-	9.37	1.11	37%	1%
28	0.95	21.28	0.011	0.11	Cl^-	9.37	1.67	83%	50%
29	0.90	49.72	0.011	0.17	Cl^-	9.34	1.74	90%	8%
30	0.57	21.28	0.011	0.15	Cl^-	5.60	1.11	81%	8%

Table S7. Batch conditions of multi-objective optimization for electrocatalytic oxidative C–C cleavage reaction.

Entry	Cat.	CatL (mg)	SubC (M)	H_2OL (%)	T (h)	E (V)	Yield (%)	FE (%)
1	Ni	2.00	0.015	10.00	20.00	1.60	18.51	6.88
2	Ni-Fe	1.82	0.050	5.38	19.30	1.77	8.47	7.16
3	Ni	0.82	0.030	14.88	15.30	2.17	22.41	3.62
4	Ni-Mn	1.32	0.020	19.63	17.30	1.97	28.65	4.03
5	Ni-Co	0.32	0.040	10.13	13.30	2.37	39.19	7.86
6	Ni-Mn	0.57	0.025	3.00	14.30	2.27	43.40	8.11
7	Ni-Co	1.57	0.045	12.50	18.30	1.87	12.53	9.48
8	Ni-Fe	1.07	0.015	17.25	16.30	1.67	11.15	22.65
9	Ni	0.07	0.035	7.75	12.30	2.07	47.57	10.05
10	Ni-Mn	1.95	0.032	13.69	19.80	2.32	28.30	7.12
11	Ni-Co	0.95	0.012	4.19	15.80	1.92	52.58	7.24
12	Ni-Fe	1.45	0.042	8.94	17.80	2.12	37.21	6.64
13	Ni-Co	0.95	0.037	13.13	15.35	1.79	17.10	7.65
14	Ni-Co	0.31	0.048	5.52	13.81	1.91	39.61	13.56
15	Ni-Co	0.49	0.043	2.26	14.48	1.90	38.63	14.77
16	Ni-Mn	0.82	0.026	4.66	12.75	1.87	43.37	13.18
17	Ni-Fe	1.06	0.021	6.93	13.76	1.87	50.89	9.93
18	Ni-Fe	0.87	0.023	9.09	14.04	1.87	34.14	7.40
19	Ni	0.50	0.038	1.08	13.43	1.73	14.75	21.40
20	Ni-Mn	0.42	0.023	3.35	13.42	1.87	45.96	12.22
21	Ni-Mn	1.17	0.029	1.91	12.30	1.66	7.77	25.19
22	Ni-Fe	0.45	0.011	3.58	19.57	1.68	19.71	23.19
23	Ni-Mn	0.82	0.018	1.19	12.74	1.87	50.19	14.85
24	Ni-Fe	0.31	0.028	3.47	14.34	1.68	7.44	21.58
25	Ni-Fe	0.89	0.015	1.29	12.07	1.87	56.76	14.02
26	Ni-Co	0.98	0.021	1.18	12.93	1.68	10.95	22.96
27	Ni	0.43	0.047	7.09	14.72	2.05	38.60	8.89
28	Ni-Co	1.35	0.022	2.27	12.71	1.71	11.37	22.54
29	Ni-Fe	1.23	0.019	1.94	12.65	2.30	46.78	6.41
30	Ni	1.41	0.019	2.51	16.14	2.22	47.95	6.42

Table S8. Batch conditions of multi-objective optimization for electrocatalytic amine oxidation reaction.

Entry	Cat	CatB	Cat.	SubC(M)	BasC	t (h)	E (V)	Yield (%)	FE (%)	Rate(mmol /cm^2/h)
1	Ni-Mn	Ni foam	K^+	0.033	1.00	3.00	0.60	94.13	96.09	0.0860
2	Ni-Co	Carbon	Na^+	0.276	0.61	3.72	0.88	21.37	84.25	0.2380
3	Ni	Carbon	Na^+	0.140	0.28	1.88	0.62	5.80	100.00	0.0650
4	Ni-Co	Ni foam	K^+	0.049	0.44	0.92	0.60	7.80	99.62	0.0620
5	Ni-Fe	Carbon	K^+	0.225	0.77	0.73	0.79	5.96	100.00	0.2760
6	Ni-Fe	Ni foam	Na^+	0.207	0.50	3.38	0.57	4.94	100.00	0.0450
7	Ni	Ni foam	K^+	0.239	0.50	1.41	0.85	12.16	100	0.3096
8	Ni-Mn	Ni foam	Na^+	0.244	0.96	2.08	0.87	19.08	100.00	0.3367
9	Ni-Mn	Carbon	K^+	0.122	0.50	3.63	0.84	73.78	100.00	0.3729
10	Ni-Co	Carbon	K^+	0.200	0.86	3.75	0.58	23.83	100.00	0.1903
11	Ni-Co	Ni foam	Na^+	0.287	0.44	0.59	0.51	1.45	100	0.1058
12	Ni-Fe	Ni foam	K^+	0.079	0.68	3.67	0.88	100.00	84.42	0.2142
13	Ni-Co	Ni foam	K^+	0.152	0.86	3.16	0.61	25.32	100.00	0.1828
14	Ni	Carbon	Na^+	0.073	0.52	3.78	0.85	87.68	73.86	0.2549
15	Ni-Fe	Carbon	Na^+	0.032	0.36	2.86	0.79	77.78	68.52	0.1294
16	Ni-Fe	Carbon	K^+	0.122	0.53	3.15	0.84	55.63	100.00	0.3240
17	Ni-Fe	Ni foam	K^+	0.127	0.50	1.99	0.82	37.89	98.93	0.3638
18	Ni-Mn	Carbon	K^+	0.110	0.42	2.29	0.82	57.20	100.00	0.4119
19	Ni-Mn	Carbon	Na^+	0.125	0.30	2.99	0.82	53.00	100.00	0.3331
20	Ni-Co	Ni foam	K^+	0.037	0.52	1.64	0.77	100.00	99.01	0.3394
21	Ni-Mn	Carbon	K^+	0.110	0.74	2.29	0.82	68.85	97.94	0.4958
22	Ni	Carbon	K^+	0.036	0.74	2.90	0.81	73.87	49.04	0.1395
23	Ni	Carbon	K^+	0.054	0.42	3.33	0.79	83.30	85.4	0.2020
24	Ni-Mn	Carbon	K^+	0.110	0.48	3.33	0.84	59.48	95.56	0.2949
25	Ni-Mn	Ni foam	Na^+	0.074	0.61	2.20	0.84	43.24	98.09	0.2168
26	Ni-Mn	Carbon	Na^+	0.077	0.81	3.02	0.81	80.60	81.8	0.3101
27	Ni	Carbon	Na^+	0.099	0.68	1.94	0.81	69.48	100.00	0.5312
28	Ni-Mn	Carbon	K^+	0.097	0.81	3.35	0.76	73.31	94.3	0.3180
29	Ni-Mn	Carbon	K^+	0.104	0.70	2.31	0.76	52.32	100.00	0.3547
30	Ni-Co	Carbon	K^+	0.097	0.49	2.84	0.82	53.72	76.49	0.2749

References

[1]. Liu, M.; Zhang, Z.; Yan, J.; Liu, S.; Liu, H.; Liu, Z.; Wang, W.; He, Z.; Han, B., Aerobic Oxidative Cleavage and Esterification of C(OH)–C Bonds. *Chem* **2020,** 6, 3288-3296.
[2]. Zhou, H.; Li, Z.; Xu, S. M.; Lu, L.; Xu, M.; Ji, K.; Ge, R.; Yan, Y.; Ma, L.; Kong, X.; Zheng, L.; Duan, H., Selectively Upgrading Lignin Derivatives to Carboxylates through Electrochemical Oxidative C(OH)-C Bond Cleavage by a Mn-Doped Cobalt Oxyhydroxide Catalyst. *Angew. Chem. Int. Ed.* **2021,** 60, 8976-8982.
[3]. Jun-Yu, Z.; Chuan, X.; Hao-Fan, W.; Cheng, T., Recent advances in electrocatalytic oxygen reduction for on-site hydrogen peroxide synthesis in acidic media. *J. Energy Chem.* **2022,** 67, 432-450.
[4]. Bawareth, B.; Di Marino, D.; Nijhuis, T. A.; Wessling, M., Unravelling Electrochemical Lignin Depolymerization. *ACS Sustainable Chem. Eng.* **2018,** 6, 7565-7573.
[5]. Marino, D. D.; Jestel, T.; Marks, C.; Viell, J.; Blindert, M.; Kriescher, S. M. A.; Spiess, A. C.; Wessling, M., Carboxylic Acids Production via Electrochemical Depolymerization of Lignin. *ChemElectroChem* **2019,** 6, 1434-1442.
[6]. Schutyser, W.; Renders, T.; Van den Bosch, S.; Koelewijn, S. F.; Beckham, G. T.; Sels, B. F., Chemicals from lignin: an interplay of lignocellulose fractionation, depolymerisation, and upgrading. *Chem. Soc. Rev.* **2018,** 47, 852-908.
[7]. Huang, J.; Jian, Y.; Zhou, M.; Wu, H., Oxidative C−C bond cleavage of lignin via electrocatalysis. Front. Chem. **2022,** 10, 1007707.